

Techniques of self-interference incoherent digital holography

Invited Paper

David C. Clark and Myung K. Kim

Department of Physics
University of South Florida
Tampa, U.S.A.
dcclark@mail.usf.edu

Abstract—We discuss and demonstrate our recent developments using self-interference incoherent digital holography to bridge the gap between indispensable incoherent imaging techniques and the advantages of three-dimensional photographic recording. We demonstrate the ability to record broadband sunlit photographic holograms, apply non-invasive three-dimensional tracking techniques, and the ease of adaptation to existing tools in microscopy and fluorescence.

Keywords— *incoherent holography; differential imaging; fluorescence microscopy; three-dimensional tracking*

I. INTRODUCTION

Image recording using incoherently illuminated objects and specimens is widely used due to immediate and low cost source light availability. Without the use of techniques such as confocal point scanning, however, only two-dimensional (2D) images are captured. In contrast, holography records sufficient information to recreate the three-dimensional (3D) optical field emanating from the scene, including both amplitude and phase [1]. The three-dimensional recording is made possible by the interference of the object's optical field and a reference optical field, and therefore requires coherence between the two. In D. Gabor's original conception, the reference is realized from a part of the illumination undisturbed by the object [2]. The invention of the laser made it possible to provide a coherent reference field explicitly [3]. Because coherence is at the core of holography, recording holograms under incoherent illumination has been problematic until recent advancements.

The introduction of Fresnel incoherent correlation holography (FINCH) has fully demonstrated the ability to generate holographic images of incoherent object fields, including 3D fluorescence microscopy [4,5]. In this technique, two copies of the object wave are superposed with different phase factors imposed by a spatial light modulator (SLM), so that every point source on the object produces the Fresnel zone interference pattern [6]. We have since developed a technique conceptually similar to FINCH called self-interference incoherent digital holography (SIDH), in which

the SLM is replaced by a modified Michelson interferometer with a differential phase curvature applied by its two mirrors [7]. For continuous objects or scenes, the spatial incoherence of the object points leads to rapid build-up of incoherent background which is removed by standard phase-shifting digital holography [8]. The resultant hologram can then be numerically propagated to any distance to reconstruct the desired optical field. Because coherence length is inversely proportional to bandwidth, broadband incoherent illuminated subjects present a notable challenge which is overcome by our SIDH process.

We discuss here our recent developments related to our method of SIDH including 3D photographic holography, differential self-interference incoherent digital holography (diff-SIDH), and holographic microscopy all involving completely spatially incoherent illumination. We first fully demonstrate SIDH and diff-SIDH on photo-quality holograms of unfiltered broadband natural sunlit objects. We then demonstrate the easy adaptation to commercial grade microscopy equipment, successfully converting a professional 2D imaging instrument into a powerful 3D imaging and

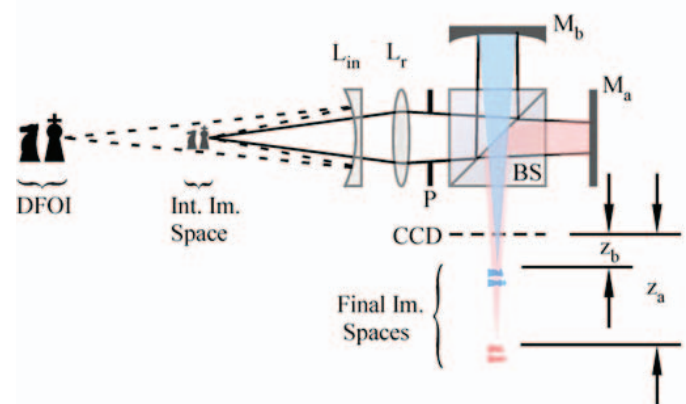


Fig. 1. Experimental diagram for diff-SIDH. An input lens, L_{in} , projects objects in the depth field of view, DFOI, into the intermediate image space as input to the SIDH module. The SIDH module consists of a relay lens, L_r , an iris, P , a beam splitter, BS, a flat piezo-mounted mirror, M_a , a curved mirror, M_b , and a CCD camera.

tracking tool.

II. EXPERIMENTS

A. Self-interference Incoherent Digital Holography

A basic SIDH configuration is represented in Fig. 1. It consists of the input lens, the relay lens, the interferometer, and a CCD array. The input lens produces an intermediate image space as the input for the SIDH module. The relay lens is selected and positioned to create an appropriate final image space relative to the CCD plane. The interferometer consists of a beam-splitting cube and two mirrors. One is a plane mirror mounted on a piezo-actuator, which is driven by a 5 volt ramp signal for phase-shifting. The other is a curved mirror to generate differential phase curvature.

To ensure interference, the distances of the two mirrors are matched to within a margin based on the temporal coherence of the desired light source [9]. The degree of this adjustment is

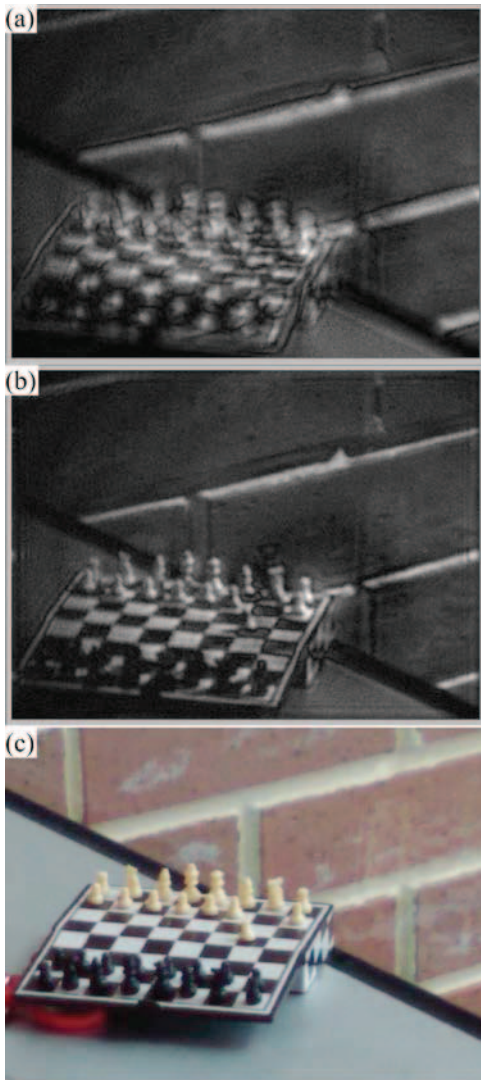


Fig. 3. Sunlit holographic recording of chess set. (a) Out of focus hologram. (b) Same hologram numerically propagated to in-focus plane. (c) Cell phone camera image of same scene for comparison.

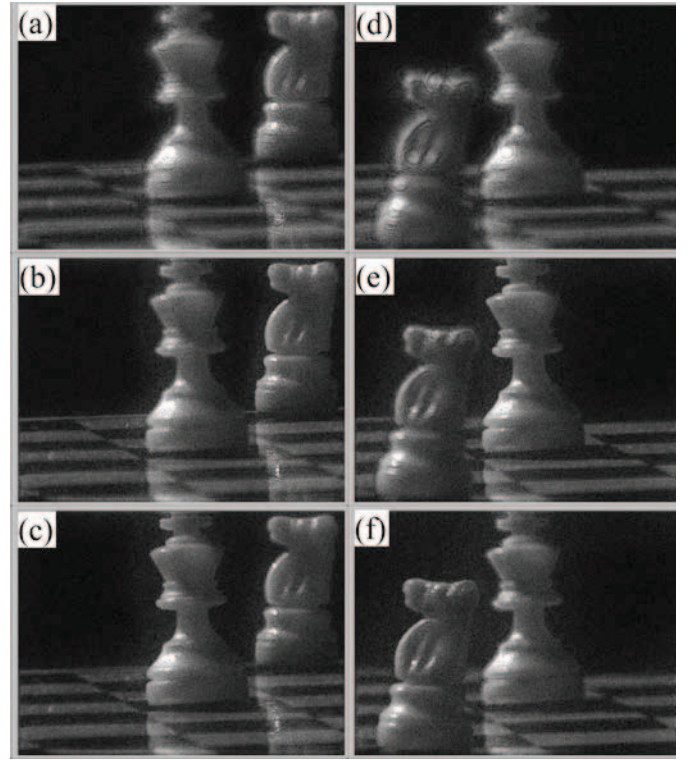


Fig. 2. Initial and final complex holograms. Chess pieces, knight and king, were arranged as shown in the initial hologram, (a-c). The knight was then moved to a new position and a final hologram was recorded, (d-f). (a), (b), and (c) are the same initial hologram at the zero-plane (un-propagated), the knight plane, and the king plane, respectively. (d), (e), and (f) are the final hologram at the zero-plane, the king plane, and the new knight plane, respectively.

visibly verified by imaging a single incoherent, out-of-focus, LED source for best fringe contrast. Then, several exposures of an incoherent illuminated scene are captured while the phase-shifting piezo-mounted mirror travels through at least one full 2π phase excursion. The complex hologram is calculated from these N intensity profiles, I_n , by

$$H = \frac{1}{N} \sum_{n=0}^{N-1} I_n e^{i2\pi \frac{n}{N}}. \quad (1)$$

It is this zero-plane (CCD-plane) complex hologram, now devoid of DC and virtual twin images, that is used for further processing, such as diff-SIDH or propagation to reconstruction planes. A minimum of $N = 4$ is required to eliminate the unwanted terms; however, using higher values (up to 20 in cases presented here) ensures removal of DC signal and smooths random noise effects. While a detailed description of the reconstruction is available in [7], we will summarize here that our resulting complex holograms are simply propagated, as per diffraction theory, by desired distances, z_h , described by

$$z_h = -\frac{z_a z_b}{z_a - z_b} \quad (2)$$

where $z_{a,b}$ are the axial positions of the final focal planes of a desired object plane through the two paths of the interferometer and are measured relative to the CCD plane.

For a well-defined system, these values are easily translated from object space to final image space and back again. For our purposes here, we use thin lens approximated geometry, as well as compensation for image shift due to the 25.4 mm BK-7 beam cube. An example of a broadband, sunlit hologram recorded using SIDH is shown in Fig. 2 numerically propagated to and out-of-focus plane (a) and the in-focus plane (b) and a cell phone camera photo (c) is included for comparison.

B. Broadband Differential Incoherent Holography

The process of diff-SIDH is applied here to the case of chess pieces on a chess board illuminated by sunlight through an office window. A hologram is recorded of the initial scene, Fig. 3(a-c). The knight was then moved to a new position and a final hologram was recorded, Fig. 3(d-f). The difference hologram is calculated from the un-propagated initial and final complex holograms (Fig. 3(a) and (d), respectively),

$$\Delta H = H_i - H_f. \quad (3)$$

The resulting difference hologram for this experiment is shown in Fig. 4(a-c) and contains the 3D optical field information of the knight in both initial and final positions, while the unchanged information, including the stationary king, are absent. As is shown, we numerically shift the focus of each hologram from initial knight to king to final knight positions (figure 4(a-c), respectively) to demonstrate that the 3D information is preserved. It can also be noticed that the information on the chess board, both overlap and specular reflection of the knight, is also preserved in a difference hologram, since this represents changed information as well.

From this single complex operation, the overall volumetric change of source points making up the scene is computed and movement of object points in the scene is tracked in three dimensions. In the present case, if we select the eye of the knight as an easy point of reference, a 3D displacement vector can be calculated showing the projected path between the time of the initial and final holograms. Using the plane parallel to the CCD plane that contains the initial eye as our reference and setting the origin at the center of our field of view (FOV), position vectors can be constructed from our difference hologram for the initial and final eye positions by

$$\mathbf{v}_i = \left[\frac{px_i}{nx} x_i, \frac{py_i}{ny} y_i, z_i \right] \quad (4)$$

where px and py are the lateral pixel position coordinates, nx and ny are the lateral FOV's in pixels, and x_i and y_i represent the object space FOV's in units of length. This object space FOV is, of course, scaled based on the depth plane of interest at z_i by the relation

$$x_i = x_0 \left(\frac{z_0 - z_i}{z_0} \right) \quad (5)$$

(and identically for y_i) where x_0 is the known object space FOV at a plane located at z_0 , and z_i is measured from this z_0 plane and is translated from z_h as described in the following paragraph. For our example, applying (4) and (5), we have

$$\begin{aligned} \Delta \mathbf{v} &= \mathbf{v}_2 - \mathbf{v}_1 \\ &= [-5.4, 2.5, 62] \text{ mm} - [8.9, 7.1, 0] \text{ mm} \\ &= [-14.3, -4.6, 62] \text{ mm} \end{aligned}$$

for the knight's displacement vector in object space.

It is important to consider the relative locations of subjects of interest, i.e., the depth field of interest (DFOI). Since we are interested in tracking objects in a 3D volume of space, our intermediate image space should consist of an appropriate volume of space as input for the diff-SIDH system. In the above experiment, the DFOI (spanning the length of the chess board) is between 350 mm and 430 mm from the relay lens. By thin lens geometry, this translates to a 2.2 mm range in intermediate image space using a negative 75 mm input lens placed 7 mm in front of the relay lens. Following similarly, the positive 50 mm relay lens of the SIDH module translates this input to a range of z_a (plane mirror path) and z_b (curved mirror path) values of 25.7 to 39.8 mm and 7.62 to 17.4 mm, respectively. Thus applying (2), we expect objects in our DFOI

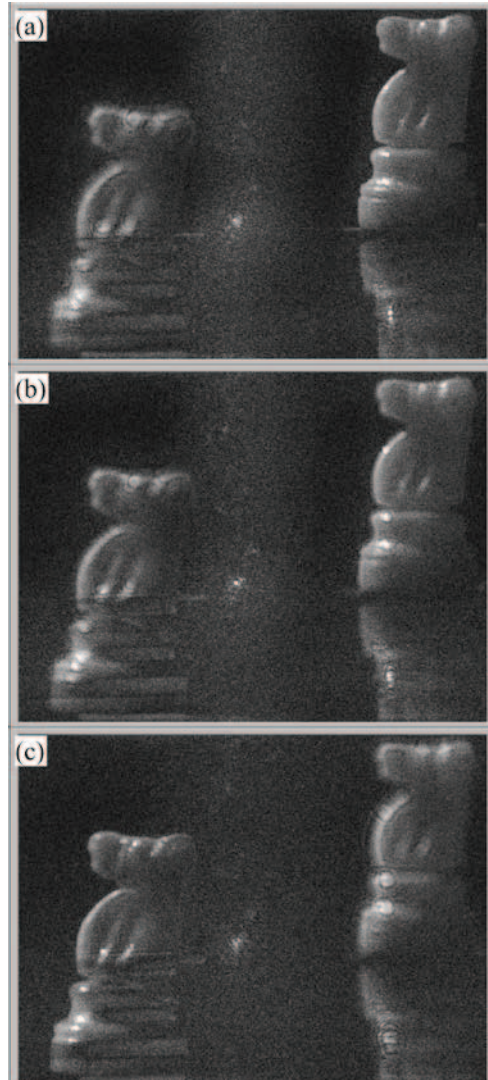


Fig. 4. Differential hologram containing the 3D information of the changes only. (a) Numerically propagated to the initial knight plane, (b) to the king plane (now absent), and (c) to the final king plane.

to come into focus somewhere within the propagation range of -10.8 to -30.8 mm. Of course, these relationships are non-linear and a numerical simulation of our constructed system produces a translation from object space DFOI into final holographic propagation space as plotted in Fig. 5. Specifically, our three object positions of interest consisting of the 425 mm initial knight position, the 401 mm king position, and the 363 mm final knight position are predicted to be in focus at propagation distances; -11.7, -16.3, and -26.4 mm, respectively. These three predicted propagation planes were chosen for display in Fig. 3 and Fig. 4. Clearly, these are appropriate planes for the objects in question.

C. Microscopic Differential Incoherent Holography

We have fabricated a similar system to that above (Fig. 1) which we mount directly to the camera port of a standard commercial microscope. In essence, the input lens is replaced by the microscope as the input device to create the intermediate image space. In this way, the bright-field microscope images are successfully recorded here as complex holograms containing the 3D volumetric information of the object space extending above and below the microscope's normal input plane.

A slide containing a USAF1951 resolution target was placed on the microscope stage while a coverslip containing two particle-like structures was held approximately 8 mm above by a separate translation stage. The volume space was illuminated by a single color incoherent LED and an initial hologram was recorded. The two-particle system was then translated laterally and a final hologram was recorded. Just as above, a difference hologram was calculated resulting in a hologram containing only the two-particle system in its initial and final positions while all unchanged information from all planes in the space is absent.

A summary of this experiment appears in Fig. 6. Fig. 6(a-c) shows the amplitude representation of the initial, final, and difference holograms, respectively, all propagated to the resolution target plane. It is obvious in the difference hologram that this plane is now devoid of the resolution target information and that only the out-of-focus projections of the translated two-particle system are present. Meanwhile, Fig. 6(d-f) contain these same three amplitude holograms, but now propagated to the particle plane. At this plane, the two-particle system is clearly identified, in-focus, in the difference hologram at both its initial and final positions even though the

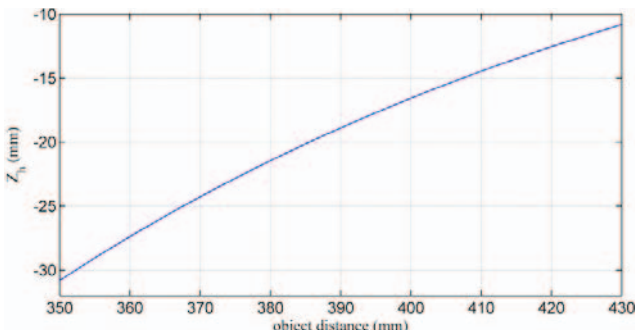


Fig. 6. Numerical simulation showing the holographic propagation distances, z_h , expected for object planes within the DFOI.

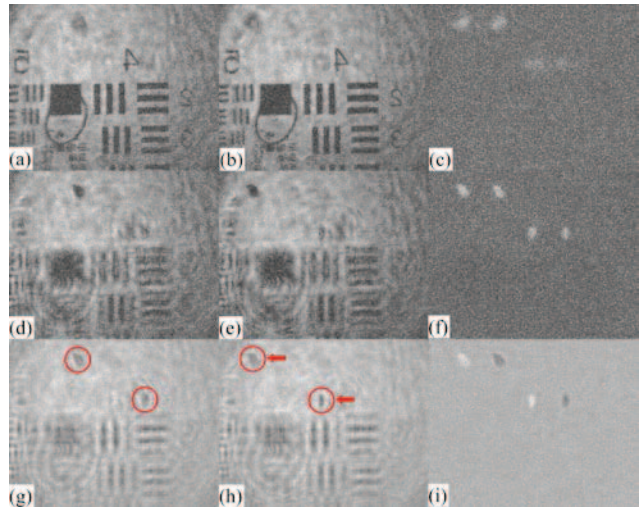


Fig. 5. Summary of differential incoherent holographic microscopy experiment. (a), (b), and (c) are the initial, final, and differential holograms, respectively, all propagated to the resolution target plane. (d), (e), and (f) are the initial, final, and differential holograms propagated to the particle plane. (g), (h), and (i) are the imaginary component images of the initial, final, and differential holograms at the particle plane showing a relative shift (to white) in the profile representing the final particle positions.

lower particle was partially obstructed by the resolution target. We point out here; information to decipher the initial and final positions of moved objects is preserved in the complex difference hologram, although this is hidden in an amplitude representation. In this case, we display in Fig. 6(g-i) only the imaginary component of each of these same holograms and propagate them once again to the particle plane. In this representation, it is easy to detect the two particles, identified by circles for convenience, in their initial positions in Fig. 6(g), and their final positions in Fig. 6(h). More importantly, in the difference hologram, Fig. 6(i), the final position of this two-particle system is shifted in this representation, clearly distinguishing it from the un-shifted initial position.

III. DISCUSSION AND CONCLUSION

We have demonstrated that our SIDH process can bridge the gap between 3D holographic imaging and existing incoherent imaging technologies. We specifically aim to combine our techniques with the versatile functional imaging of fluorescence microscopy. In this way, we will record 3D fluorescence profiles and track fluorescent tags in living organisms without the use of phototoxic raster scanning of point detection [10]. Additionally, we aim to improve measurement precision of biological cell traction force previously measured by quantitative phase imaging of surface wrinkles caused by cellular movement [11]. A deformable gel could be labeled with fluorescent beads tracked by differential fluorescence holography after cellular motion across the substrate as outlined in Fig. 7.

We are also currently developing a single-shot, off-axis SIDH method which will eliminate the need for phase-shifting by incorporating a slight tilt between the self-interfering copies [12]. This may be quite significant for dynamic biological applications where temporal resolution is important as well as

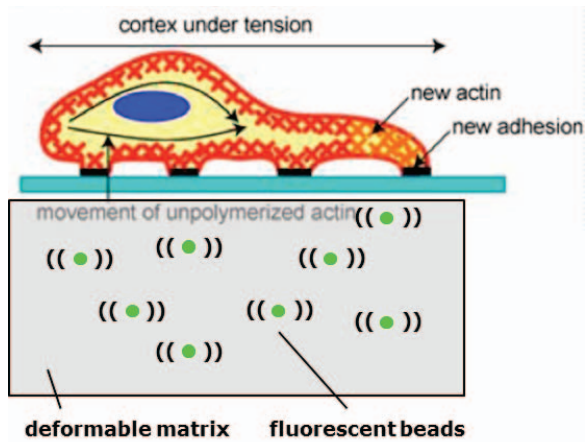


Fig. 7. Deformable stuff like previous wrinkles. fluor beads in deformable matrix. DHFM with mechanical deformation (how?). crawling cells cultured on top surface.

vastly improved frame rates for 3D holographic video photography.

ACKNOWLEDGMENT

We would like to thank Dr. Byeong Cha from the Department of Molecular Pharmacology & Physiology of University of South Florida Morsani College of Medicine for his helpful input on biological and fluorescence applications.

REFERENCES

- [1] Hariharan, P., [Optical Holography: Principles, Techniques, and Applications], Cambridge University, (1996).
- [2] Gabor, D., "A new microscopic principle," *Nature* 161(4098), 777–778 (1948).
- [3] Leith, E. N. and Upatnieks, J., "Wavefront reconstruction with continuous-tone objects," *J. Opt. Soc. Am.* 53, 1377–1381 (1963).
- [4] Rosen, J. and Brooker, G., "Non-scanning motionless fluorescence three-dimensional holographic microscopy," *Nat. Photonics* 2, 190–195 (2008).
- [5] Rosen, J. and Brooker, G., "Fluorescence incoherent color holography," *Opt. Express* 15, 2244–2250 (2007).
- [6] Rosen, J. and Brooker, G., "Digital spatially incoherent Fresnel holography," *Opt. Lett.* 32, 912–914 (2007).
- [7] Kim, M. K., "Incoherent digital holographic adaptive optics," *Appl. Opt.* 52, A117–A130 (2013).
- [8] Yamaguchi, I. and Zhang, T., "Phase-shifting digital holography," *Opt. Lett.* 22, 1268–1270 (1997).
- [9] Dubois, F., Callens, N., Yourassowsky, C., Hoyos, M., Kurowski, P., and Monnom, O., "Digital holographic microscopy with reduced spatial coherence for three-dimensional particle flow analysis," *Appl. Opt.* 45, 864–871 (2006).
- [10] Lorbeer, Raoul-Amadeus, et al., "Highly efficient 3D fluorescence microscopy with a scanning laser optical tomograph," *Opt Express* 19, 5419–5430 (2011).
- [11] Yu, Xiao, et al., "Measurement of the traction force of biological cells by digital holography," *Biomed Opt Express* 3, 153–159 (2012).
- [12] Hong, J. and Kim, M. K., "Single-shot self-interference incoherent digital holography using off-axis configuration," *Opt. Lett.* 38, 5196–5199 (2013).